Research article

Preparation and characterization of clay based ceramic porous membranes and their use for the removal of lead ions from synthetic wastewater with an insight into the removal mechanism

Abdelrahman K.A. Khalil [a], Abdelaziz Elgamouz [a,b,**], Saad Nazir [c], Muataz Ali Atieh [a,d], Hussain Alawadhi [a,e], Tahar Laoui [a,c,*]

[a] Research Institute of Sciences and Engineering (RISE), University of Sharjah, Sharjah, P.O. Box 27272, United Arab Emirates
[b] Department of Chemistry, College of Sciences, University of Sharjah, Sharjah, P.O. Box 27272, United Arab Emirates
[c] Department of Mechanical and Nuclear Engineering, College of Engineering, University of Sharjah, Sharjah, P.O. Box 27272, United Arab Emirates
[d] Chemical and Water Desalination Engineering (CWDE) Program, College of Engineering, University of Sharjah, Sharjah, P.O. Box 27272, United Arab Emirates
[e] Department of Applied Physics & Astronomy, University of Sharjah, P.O. Box 27272, Sharjah, United Arab Emirates

A B S T R A C T

The present study explores the use of local clay from the United Arab Emirates (UAE) to prepare porous ceramic membranes (flat disk shape) for the purpose of removing toxic heavy metals from contaminated water. Four distinct ceramic membranes, crafted from locally sourced clay and incorporated with activated carbon and graphite, underwent careful and thorough preparation. The initial set of membranes was subjected to open-air sintering, resulting in the creation of mACA and mGrA membranes. Concurrently, a second set of meticulously prepared membranes underwent sintering under inert nitrogen conditions, yielding the formation of mACI and mGrI membranes, respectively. Prior to making the membranes, the clay material was characterized by thermogravimetric analysis (TGA), X-ray fluorescence (XRF), Fourier-transform infrared spectroscopy (FTIR), and X-ray diffraction analysis (XRD). The clay presented the lowest weight loss compared to AC and Gr, implying that these two materials could be used as porogen agents. The X-ray fluorescence results indicated that the natural clay contained 65.5 wt% of silicon dioxide (SiO_2), aluminium oxide (Al_2O_3), and iron (III) oxide (Fe_2O_3) falling within the class C category of clays according to ASTM. The FTIR analysis showed different clay regions allocated to various stretching and deformation vibrations of hydroxide, organic fraction, and (Si, Al, Fe)–O groups. The XRD analysis revealed the presence of kaolinite, illite, smectite and calcite phyllite phases in the clay mineral. The membranes were characterized using FESEM, with those containing AC (used as porogen) exhibiting large pores clearly visible on the surface, and were tested for the removal of lead (Pb^{2+}) ions from synthetic wastewater. The removal efficiencies of the membranes were 33 %, 75.2 %, 100 % and 100 % for mACA, mACI, mGrA and mGrI respectively after 100 min operation. The wettability of the membranes was found to follow the order mACI < mACA < mGrI < mGrA, which corroborated well with water fluxes of 7, 8, 112 and 214 L h^{-1} m^{-2} recorded after 60 min duration and 1.0 bar applied pressure. The mechanisms of filtration of

---

* Corresponding author. Department of Mechanical and Nuclear Engineering, College of Engineering, University of Sharjah, Sharjah, P.O. Box 27272, United Arab Emirates.
** Corresponding author. Department of Chemistry, College of Sciences, University of Sharjah, Sharjah, P.O. Box 27272, United Arab Emirates.
E-mail addresses: aelgamouz@sharjah.ac.ae (A. Elgamouz), tlaoui@sharjah.ac.ae (T. Laoui).

Pb^{2+} ions were adsorption for the AC-based membranes (mACA, mACI) and a combination of adsorption and size exclusion for the Gr-based membranes (mGrA, mGrI).

1. Introduction

Water is one of the most vital resources for maintaining life on our planet. All living organisms, including animals and plants, cannot survive without it, and supplying enough clean water is essential for the environment and health. With the increase in the world population accompanied by urbanization and industrialization, the gap between the limited water resources and the demand increases continuously, increasing the pressure on natural systems to supply enough clean water. This creates a significant challenge that many countries face today. Water treatment can enhance the economy by reducing the funds spent on environmental issues and project initiatives. Industrial wastewater treatment using conventional methods is more effective and cheaper than water desalination; the treated wastewater can be used in agriculture. When present at an unacceptable concentration, toxic heavy metals can negatively impact survival, reproduction, or at times behavior [1]. Among them, lead (in the form of Pb^{2+} ions) is used in many applications, such as rolled extrusion, ammunition, pigment, cable sheathing, and batteries, with the latter being the principal source of lead consumption. Pb^{2+} is mainly used in lead-acid batteries in automobiles, accounting for 80 % of this industry. Pb^{2+} based batteries are also made for planes, tanks, trains, tractors, and other heavy machines. It has also been proven to be a good shield for radiation in hospitals for the administration of some radioactive drugs, such as Technetium for leaver diagnosis and Iodine 127 for thyroid diagnosis. Lead has been used in such extensive ways because it is corrosion resistant. The large use of Pb metal has produced large amounts of contaminated wastewater. For example, acid reclamation is the only complex process that generates many chemicals during the recycling of lead batteries. Other processes are straightforward, plastic, and secondary lead regenerations. Therefore, it is essential to explore new methods of separating and recovering this metal in its dissolved form from the environment. Many methodologies have been used for Pb^{2+} removal; the adsorption, coagulation, and flocculation are among the widely used techniques [2,3]. Furthermore, ceramic membranes have proven to be strong mechanically, thermally, and stable compared to other membrane categories. They can work in aggressive media, such as the acid reclaiming process in batteries.

Membrane processes have been broadly used in several industrial applications in recent decades, including wastewater treatment or desalination of seawater [4,5], the petrochemical industry such as crude petroleum, natural gas, and dehydrogenation processes [6–8], food industry, and pharmaceutical sector [9–12]. Membrane techniques have lately become popular due to their appealing benefits, such as high separation efficiency. Microfiltration (MF), for example, is the only membrane process that can treat a large volume of liquid at low transmembrane pressure (less than 2 bar) due to its high flux compared to other membrane processes [13]. MF is regarded as an effective turbidity removal process, in addition to being cost-effective. Furthermore, MF is an environmentally friendly separation process that may be used at a relatively cheap cost in various environmental applications. Ceramic-based materials shaped into membranes have proven to be efficient and cost-effective when used to treat wastewater compared with polymeric membranes [14–19]. Characterized by their robustness, thermal stability, and capacity to withstand in aggressive media, ceramic membranes are commonly used to decontaminate industrial effluents from toxic heavy metals [1,20–24]. Ceramic membranes can bypass coagulation, flocculation, sedimentation, photocatalysis and many other forms of effluent treatment. Ceramic membranes can be prepared from metal oxides such as titania, alumina, zirconia, silica, as well as glassy materials. Ceramic membranes have been prepared in different shapes, including plate and frame, tubular, capillary, and hollow fiber. Tubular and planar filtration membranes are the most utilized shapes of membranes for the reason that they are presented with additional operating factors namely the flux and removal efficiency. On the other hand, clay materials are largely available minerals that have been used since the millennia to make clay pots and kitchen wares. Clays are presented with many characteristics that cannot be found in other minerals such as elasticity and anisotropy and being able to compact without a need of binders. Filtration through membranes is controlled by many parameters such as degree of hydrophobicity, surface charge, and pores' size/structure.

The aim of this work is to fabricate a low-cost ceramic MF membrane from natural UAE clay via the powder metallurgy method, and to assess its performance for the removal of Pb^{2+} ions from synthetic polluted water.

2. Materials and methods

2.1. Materials

Local clay was collected from Hajjar mountain in Ras Al Khaimah-UAE and brought to the lab in the form of chunks. Charcoal activated carbon was obtained from PANREAC AppliChem and ITW Reagent Ltd., Barcelona, Spain. Graphite powder with 300 nm particle size and 99.95 % purity was acquired from Changsha Easchem Co., Limited, Hong Kong, China. Clay, activated carbon, and graphite powders were used without any further purification. Lead nitrate (Pb(NO$_3$)$_2$) was purchased from Honeywell Riedel-de Haën (Germany). MilliQ ultra-pure water with a resistivity of 17.5 MΩ (Fisherbrand Accu20 Ultrapure Water System, Loughborough, UK) was used for the preparation of all solutions and also to run water flux experiments for the membranes.

2.2. Membranes fabrication

The membrane labels, sintering atmosphere, and starting materials are presented in Table 1. The grinding technique was used to

obtain the desired powder particle size range from the collected raw clay rocks using a mortar and pestle. The clay powder was made into small grains with particle size diameter $\Phi \leq 250$ μm using ASTM standardized sieves. Membranes were prepared according to the schematic diagram presented in Fig. 1. A powder metallurgical process was used to produce the four membranes mACA, mACI, mGrA and mGrI composite membranes. 5.82 g of natural clay was mixed with 0.18 g of AC or Gr to obtain mACA and mGrA respectively. No water was added to the mixtures, they were mixed manually in a glass bottle and introduced into D2 tool steel die set with 32.5 mm diameter and pressed uniaxially using a hydraulic press machine (Carver, Inc. USA) under a pressure of 14 tons.

Two disc-shaped membranes were sintered in open air to a final temperature of 1000 °C using a muffle electric furnace (NABER 2804) and following the heating program. The other two membranes mACI and mGrI were prepared from 5.82 g clay, 0.18 AC or Gr in addition to 0.12 g starch, the mixture was suspended in 25 mL of water and sonicated at room temperature for 2 h to achieve homogeneous dispersion of all components. Water was evaporated on a hot plate from the two mixtures. Fig. 1 shows a flow chart of the mixture preparation process. The AC/Clay/starch and Gr/Clay/starch mixtures were crashed into fine powder and compacted into a disc-shaped membrane using the D2 tool steel die, then sintered to 1000 °C under nitrogen atmosphere as explained in Fig. 1.

There were four steps to the thermal heating cycle: (1) heating at 250 °C for 2 h to ensure the evaporation of remaining water; (2) heating at 500 °C for 2 h to enable thermal degradation of organic matter; (3) heating at 700 °C for 2 h to facilitate the dihydroxylation of clay minerals and the decomposition of mineral carbonates; (4) sintering at 1000 °C for 2 h to ensure the densification of the ceramic membranes through reduction of porosity and strengthening the mechanical performance of the ceramic membranes. The heating rate between different plateaus was 5.0 °C/min. Flat disc membranes with 32 mm diameter and 2–3 mm thickness were obtained, as shown in Fig. 2.

2.3. Characterization

Fourier Transform Infrared spectroscopy (FTIR) of the raw materials and the sintered membranes were carried out using a PerkinElmer provided with attenuated total reflectance (ATR) unit. Spectra were recorded between 4000 and 400 cm^{-1} in the transmittance mode. Thermogravimetric analysis (TGA) was used to record the thermal phenomena that happen in the clay, activated carbon and graphite, they are accomplished using a thermal analyzer type Microbalance 2960 SDT V 3.0. The samples are heated linearly in the air from a room temperature of 21 °C–800 °C, with a heating speed of 10 °C/min. X-ray diffraction was carried out using a D8 Advance Bruker X-ray diffractometer (XRD) with a Cu Kα having a wavelength $\lambda = 1.54056$ Å as an X-ray source at a generator voltage of 40 kV and a current of 40 mA. A Field Emission Scanning Electron Microscope (FE-SEM) from Thermo scientific Apreo C was used to visualize the microstructure of the developed material, with an accelerating voltage of 15 kV. X-ray Fluorescence (XRF) was utilized to measure the chemical composition of the clay material used in the preparation of the membranes at different temperatures. An X-ray analytical microscope (XGT-7200) from HORIBA Scientific is used to get the XRF data. PE crystal (2d = 8.742 Å) analyzer, and gas flow proportional counter was used. The tube rating was 50 kV, 40 mA, and 2Ө range of 58° to 147°. The 2Ө range is found to be appropriate for main elements determination in clay using a recorder coupled detector.

2.4. Filtration experiments and Pb^{2+} detection

Filtration and water permeability tests were performed on the mACA, mGrA, mACI, and mGrI composite ceramic membranes using a customized (designed and fabricated) water flow loop system, (Fig. 3). The flow loop includes a feed-in tank, a centrifugal pump for circulation, valves, and pressure gauges to regulate the flow rate of filtration, and a customized membrane housing made of aluminum to hold the flat disc membrane, containing three inlets to allow for crossflow filtration. The high-pressure centrifugal pump moves out the Pb^{2+} polluted water at a constant water flow, and a rotameter ranging between 1: 100 LPM was used to monitor the flow. Two flow valves were used to control the flow, one at the water feed, and the other at the exit. The filtrate was collected from the membrane housing in an open atmosphere in a 50 mL test tubes every 20 min. The obtained Pb^{2+} permeate samples were analyzed by the Atomic Absorption Spectrometer (AAS, AANALYST 400, Germany), the hollow cathode lamp of single element was used to analyze Pb^{2+} at 217.0 nm wavelength. The removal% of Pb^{2+} using the mACA, mGrA, mACI, and mGrI composite membranes is determined using equation (1).

$$Removal\% = \frac{Ci - Cpr}{Ci} \times 100 \tag{1}$$

where C_i is the concentration of Pb^{2+} in ppm in the initial feed solution, and C_{pr} is the concentration in ppm of the permeate solution.

The permeate flow rate (J) in $L.m^{-2}.h^{-1}$ is mesured using equation (2).

Table 1
Labels of the prepared clay membranes along with additives and sintering atmosphere.

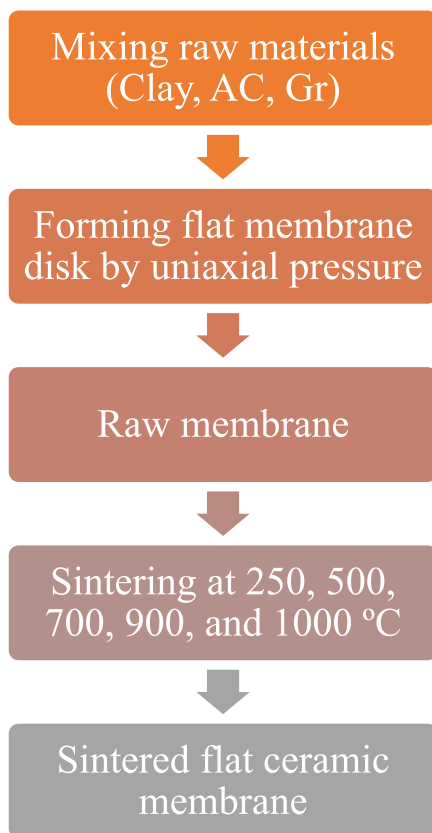| Membrane label	Additive material	Clay	Sintering atmosphere
mACA	3 wt.% AC (0.18 g)	5.82 g	Air
mACI			Nitrogen
mGrA	3 wt.% Graphite (0.18 g)	5.82 g	Air
mGrI			Nitrogen

Fig. 1. Flow diagram of ceramic membrane preparation and processing.

$$J = \frac{V}{A \times t} \tag{2}$$

where V, is the volume of the permeate, A is the membrane filtration surface, which is found to be $8.04 \times 10^{-4} cm^2$, and t is the permeation time.

The porosity of the membrane disc is crucial as it influences the membrane water flux during filtration experiments. Upon filtration, the feed water is divided into a filtered clean water and a more Pb^{2+} concentrated retentate. One pressure regulator was used to control the flow of the contaminated water. The porosity of the membrane discs was determined using the Archimedes method, after immersing the disc in water for 24 h, and the porosity of the disc was calculated using equation (3)

$$\%Porosity = \frac{M_a - M_b}{M_b} \times 100 \tag{3}$$

where M_a is the mass of the disc in gram measured after being immersed in water for 24 h, M_b is the mass of the disc in gram after drying at 100 °C.

3. Results and discussion

3.1. Characterization

3.1.1. Raw materials

The chemical composition of the natural clay used in the present study is given in Table 2. It shows that the natural clay is composed of 65.52 wt% of (SiO_2, Al_2O_3, and Fe_2O_3) falling within the range of 50–70 wt%. Therefore, this clay could be classified as class C according to ASTM C618 [25]. Si-, Ca- and Al are elements that can be found mainly in kaolinite, calcite, illite, and smectite, which are shown in the XRD pattern spectra of clay material represented in Fig. 7. The clay contains around 13.46 % iron (III) oxide (Fe_2O_3), which is within the range shown by natural clays [26]. The iron oxide content of a clay is reported to affect its color [27] and it is associated with the presence of many clay fractions such as kaolinite, illite and smectite [28]. The clay is composed of 22 wt% CaO, indicative of calcite presence, and this amount is considered to be high compared to natural clays. The presence of calcite in a clay is a
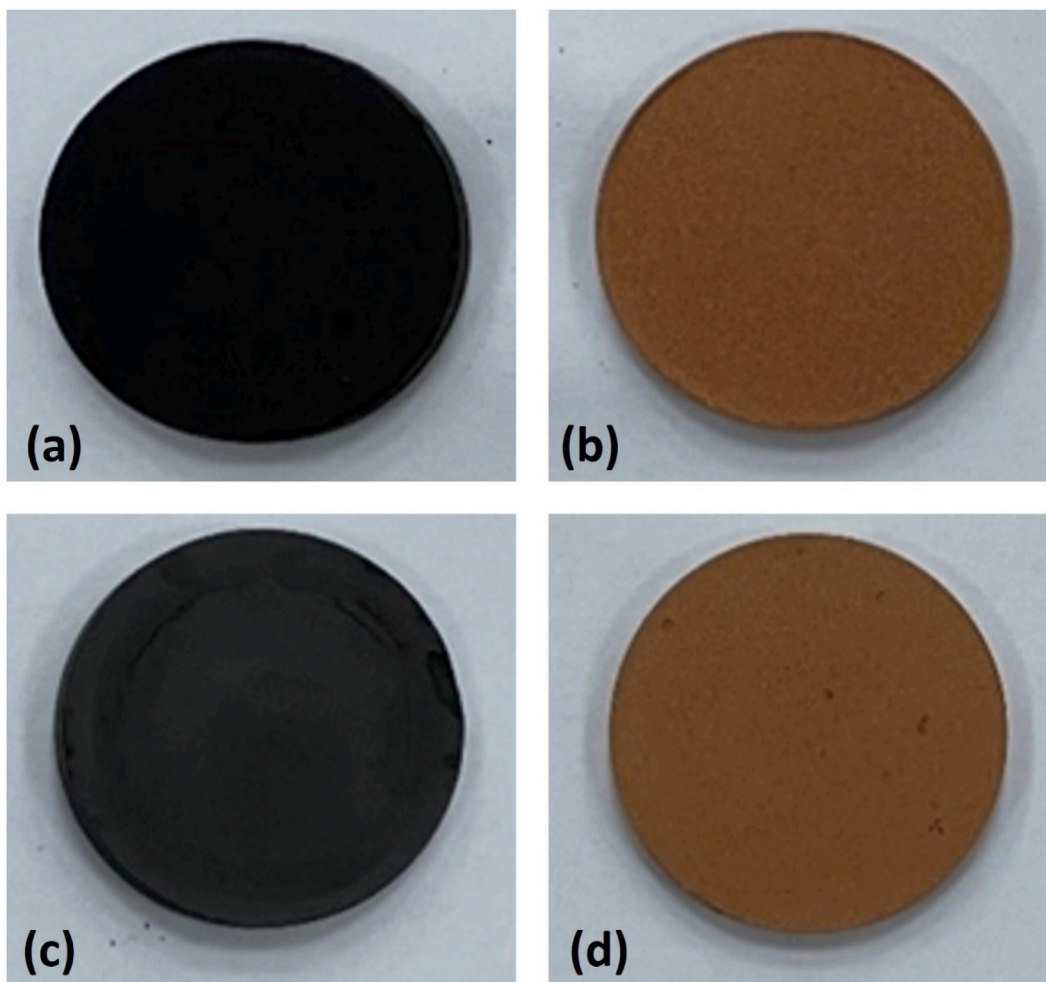
Fig. 2. Photographs of the AC and Gr composite ceramic membranes sintered at 1000 °C. (a) mACI, (b) mACA, (c) mGrI, (d) mGrA.

source of creating fissures and defects in the final specimen, thus the sintering process needs to be carried out carefully to avoid such defects and fissures. Other elements such as Mg, K, Ti, and Mn are present in the clay mineral with very low weight percent. The element Mg occupies the interstitial sites in illite and smectite phases, whereas K could occupy non-exchangeable positions because it may be held between two adjacent illite's tetrahedra [29]. The loss on ignition (LOI) presents the chemical makeup of the clay and it is found to be (19.5 wt%), indicating that the clay consists of hydrates and labile hydroxy compounds, such as kaolinite, which can be subjected to a phase change between 700 and 800 °C. It is also indicative of the presence of carbon dioxide originated from carbonates. This LOI is within the range of 18.0–32.1 % shown by natural clay minerals [29].

Thermal analysis (TGA) was carried out on the graphite, activated carbon and raw clay used for the preparation of the ceramic membranes to understand the possible transformations taking place in the ceramic specimen during the heating cycle, this being useful to design a proper sintering program for the clay membranes. It was found that varying the temperature had a direct effect on the structure of the three materials. Fig. 4 shows the TGA analysis for graphite powder, activated carbon and clay.

For the graphite powder, the weight loss started to take place at around 680 °C, as determined from the graph by the intersection of the two linear branches of TGA, and at 800 °C, all the graphite mass was lost. For the TGA of AC, a weight loss of about 16 wt% was observed between 25 and 80 °C, attributed to the loss of adsorbed water on the AC surface. Above 80 °C, the AC displayed a similar behavior to graphene with an intense weight loss of about 80 wt% at a temperature of 580 °C. The difference in the onset degradation temperatures between graphite and AC arises from their structures. Graphite has uniform, layered structure with atoms well bonded to each layer, resulting in stable sheets/layers of graphite.

However, AC has a complex lattice with no distinct or repetitive structure. This irregularity leads to many foldings in the structure creating many pores and large surface area, making it suitable for adsorption of water molecules as demonstrated by the first weight loss of 16 wt% between 25 and 80 °C. Similar results were demonstrated by Kim et al. when comparing graphite to a carbon graphite coated anode for rechargeable batteries [30]. With regard to the TGA curve of the clay material, many transformations could be identified, and a total weight loss of about 20 wt% is shown between 25 and 800 °C. The TGA could be divided into 4 different stages,
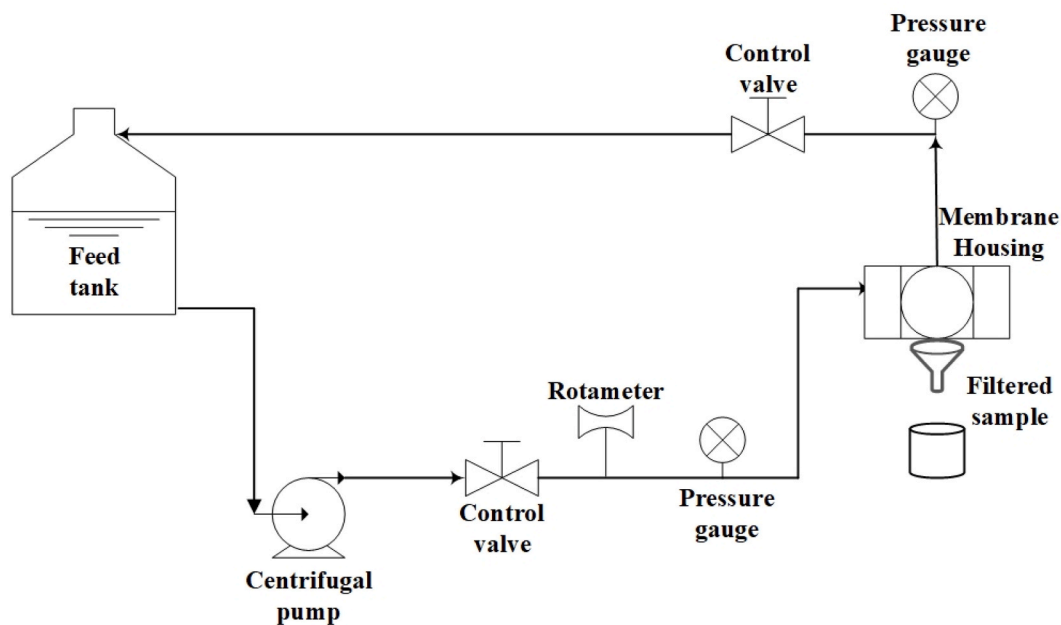
Fig. 3. Schematic diagram of the customized filtration flow loop.

Table 2
Oxides composition of the natural clay obtained using XRF analysis.

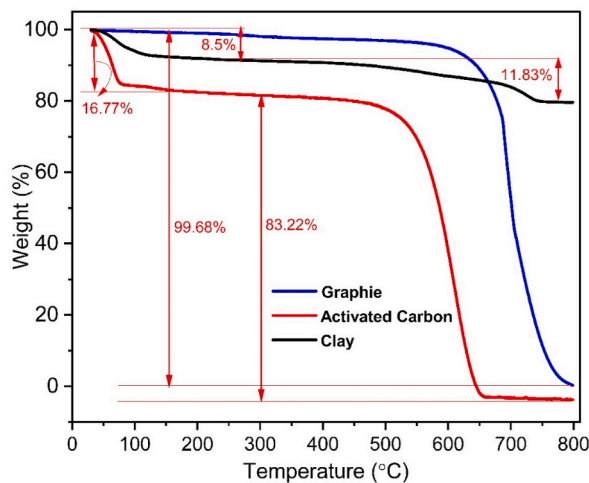| Element/oxide	Weight (%)	Element/oxide	Weight (%)
SiO_2	44.57	K_2O	0.14
CaO	22.03	Cl	0.07
Fe_2O_3	13.46	TiO_2	0.06
Al_2O_3	7.49	P_2O_5	0.13
MgO	3.99	MnO	0.008

Fig. 4. Thermogravimetric analyses (TGA) of graphite (Gr), activated carbon (AC) and raw clay mineral (powder form) used in the preparation of the membranes.

the first one between 25 and 100 °C corresponding to the surface area adsorbed water's loss. The second stage is taking place between 200 and 400 °C corresponding to combustion of organic matter present in the clay. The third phenomenon between 400 and 680 °C is due to the decarboxylation of kaolinite and illite phases [29]. The final stage between 680 and 800 °C represents the decomposition of

carbonates. Fig. 5a illustrates the FT-IR spectra of the clay mineral sintered to different final temperatures. The first assessment of the spectra indicates that the peaks in the region's features of clays (3750–3300), (3000–1800), (1450–1400), (1200–900), and (900–400) cm^{-1} are allocated to various types of stretching vibrations and deformation of hydroxide structures, organic fraction, and (Si, Al, Fe)– O groups [31]. The peak at 3750 cm^{-1} is attributed to the stretching vibrations of hydroxyl groups [32,33]. The band at 2316 cm^{-1} is attributed to vibrations of deformation of the bonds of the water molecules.

The peak between 1600 and 1700 cm^{-1} corresponds to the valency of hydroxyl ions vibrations of the water [34]. The absorption band that occurs at 1462 cm^{-1} can be attributed to the CH_2 of organic fraction bend (scissors) vibrational mode [35,36]. When high temperatures occur, OH vibrational peaks disappear due to the loss of adsorbed water. These vibrations are displayed at lower vibration in bending modes. The OH group deforming vibrations at 916 cm^{-1} are attributed to the vibration in the water interlayer. While stretching vibration of metal-oxygen stretching frequencies of iron-bearing kaolinite is depicted at peaks 841 and 874 cm^{-1} as represented in Fig. 5b [37].

3.1.2. Membranes

The microstructure morphology of membranes' surface is presented in Fig. 6. The effect of AC addition on the microstructure of the membrane can be clearly depicted when observing the micrographs.

As observed in FE-SEM image Fig. 6a of membranes with addition of AC, commixing AC with clay shows a noticeable disparity in the surface, where AC particles are found to be distributed on the surface of the hybrid clay/AC membrane (Fig. 6b), in addition to the relatively large average pore diameter. No crystals could be seen from the FE-SEM micrographs (Fig. 6c and d), which is indicative that the clay is a mixture of different phases with quartz being the major component; no defined size could also be identified for the particles. A glassy phenomenon can be observed from the micrograph of the membranes, which represents the fusion of the clay fractions platelets. This phenomenon happens when clay ceramics are treated under high temperature, which helps in the fusion of clay particles to produce a membrane with low porosity [38]. The X-ray analysis of the membranes is presented in Fig. 7. A mixture of mineral phases, such as quartz (Q), calcite (C), kaolinite (K), smectite (S), and illite (I), were identified in the sintered membranes by their 2 theta positions [29]. The three spectra presented similarities, with peaks associated with kaolinite, calcite, illite, and smectite shortened for mACA, mACI, mGrA, mGrI compared to plain clay membrane. Quartz emerged as the predominant component within the clay mineral composition. The specific interreticular distances, Miller indices, and the corresponding 2θ positions derived from diffractometric analyses exclusively pertain to quartz: 5.26, (100), 20.5°; 3.25, (101), 26.3°; 2.36, (110), 36.4°; 2.23, (200), 42.12°; and 1.71, (112), 50.3°. Additionally, a triplet was observed at 1.32, (212), 67.4°; 1.385, (203), 67.23°; and 1.27, (301), 68.16°. These quartz diffractions align with the powder diffraction file No 00-046-1045. Furthermore, the analysis identified the presence of triclinic kaolinite, characterized by specific interreticular distances, Miller indices, and 2θ positions: 7.24, (00L), 12.1°; 4.36, (020), 19.706°; 3.51, (002), 24.65°; and 2.26, (003), 37.84° [39]. The kaolinite diffractions correspond to the powder diffraction file No 00-014-0164. Illite was also discerned in the composition, and its characterization involved interreticular distances, Miller indices, and 2θ positions: 10.21, (002), 8.76°; 5.13, (004), 17.5°; and 3.31, (006), 26.4°. These illite diffractions align with the powder diffraction file No 00-026-0911.

The existence of carbonate, specifically in the form of calcite, was identified through the determination of interreticular distances, Miller indices, and the corresponding 2θ positions obtained from diffractometric analysis: 3.82, (012), 23.05°; 3.1, (104), 29.2°; and 2.71, (113), 39.2°. These distinctive calcite diffractions were cross-referenced with the powder diffraction file No 00-005-0586.

It is noteworthy that subjecting the raw material to calcination at temperatures exceeding 700 °C resulted in the disappearance of these calcite diffractions [38].
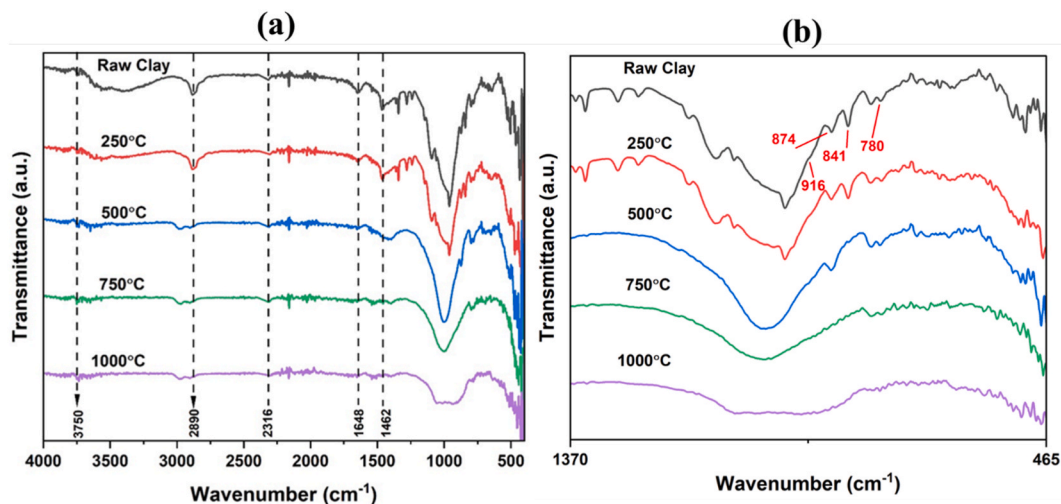

Fig. 5. (a) FT-IR spectra of raw clay material, clay heated to 250 °C, heated to 500 °C, heated to 750 °C, and heated to 1000 °C. (b) 1370-500 cm^{-1} FTIR region.
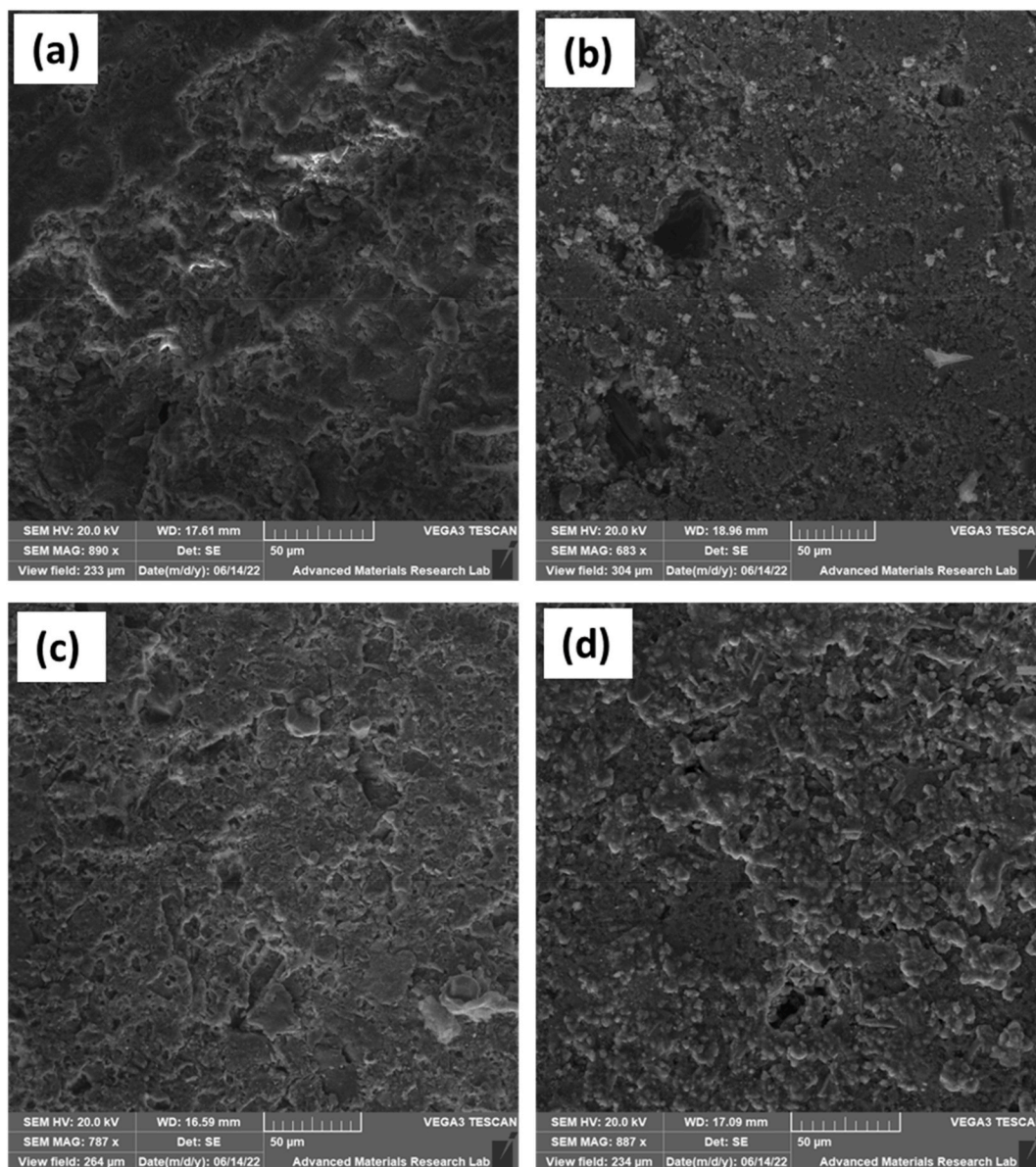
Fig. 6. FE-SEM micrographs of clay membrane discs. (a) mACA, (b) mACI, (c) mGrA, and (d) mGrI.

The N_2 adsorption/desorption isotherms of the four membranes, mACA, mGrA, mACI, and mGrI sintered to final temperature of 1000 °C, are presented in Fig. 8.

The hysteresis loops obtained for these membranes are of type H3 according to the IUPAC classification, H3 desorption branches have characteristic shoulders which cross the adsorption branch usually at lower closures points compared to other hysteresis, all hysteresis is also characterized by the absence of a plateau at higher relative pressure P/P^o. The H3 hysteresis type is characteristic for clay materials and platy particles [40]. The AC induced pores in both membranes mACA and mACI (Fig. 8a and b) are presented with very small pocket compared to the graphite induced pores membranes mGrA and mGrI (Fig. 8c and d), indicating no effect of the sintering medium on the membrane final porous structure. All membranes adopt a "slot" like pores due to the phyletic structure of the starting materials, clay as well as the graphite porogen agent. The parameters derived from the adsorption desorption of N_2 for the four membranes mACA, mGrA, mACI, and mGrI, are tabulated in Table 3. Generally, when AC is used as porogen, lower surface areas are attained, for example values of 2.00 and 3.13 m^2/g are obtained for mACA and mACI respectively. However, when graphite is used as porogen, relatively higher specific surface areas are obtained, for example, 10.0 and 3.73 m^2/g are obtained for mGrA and mGrI respectively. No trend was found for sintering the membrane in open air or inert nitrogen, high values for the surface area were obtained when sintering the porogenated AC clay membranes, while lower values were obtained for nitrogen sintered Gr porogenated membrane. Sintering in N_2 and other inert gases are usually used to avoid formation of oxides but there is no evidence they could yield
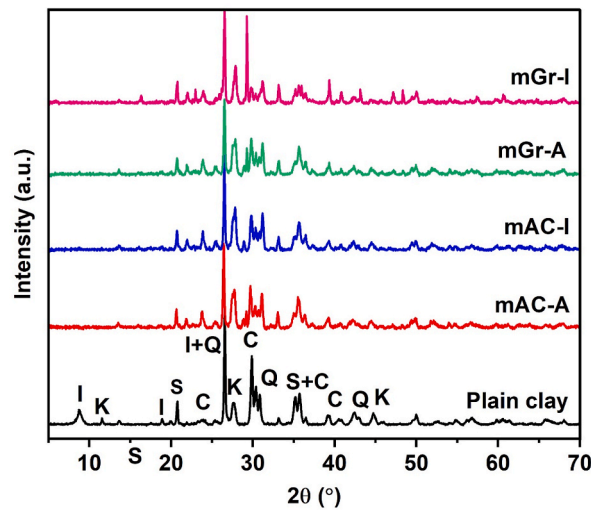
Fig. 7. X-ray diffraction of clay membranes. C: calcite, I: illite, K: kaolinite, Q: quartz, S: smectite.
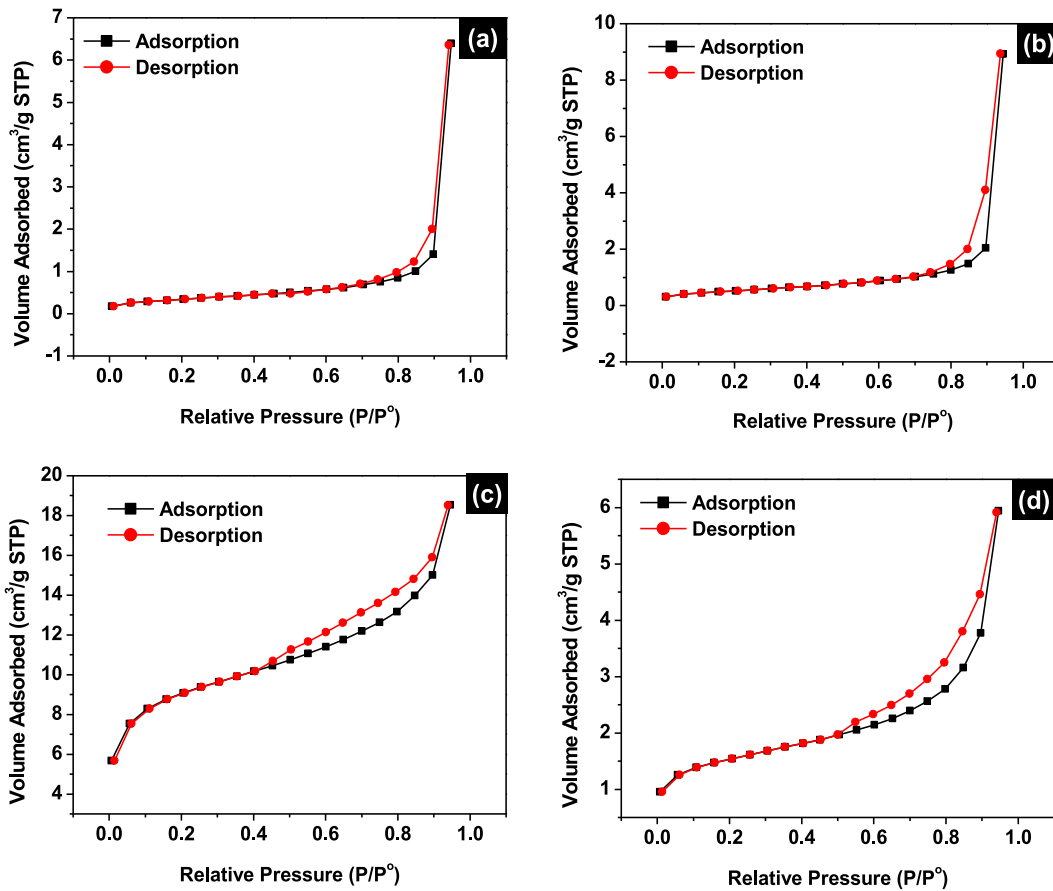

Fig. 8. Nitrogen adsorption/desorption isotherms of the membranes (a) mACA, (b) mACI, (c) mGrA, and (d) mGrI.

high surface areas [41]. The pores volumes of the four membranes mACA, mGrA, mACI, and mGrI, are found to follow the following order: 0.00858 < 0.0105 < 0.0150 < 0.0184 cm^3/g respectively, indicating no direct relationship with the surface area. The radius of the pores however seems to follow a reverse trend of the surface area, indicating that high radii are obtained when AC is used as

Table 3

Nitrogen adsorption/desorption derived structural parameters for mACA, mGrA, mACI, and mGrI composite membranes.

Membrane	Average pore radius (nm)	Specific surface area (m^2/g)	Volume of the pores (cm^3/g)	Porosity (%)
mACA	16.4	2.00	0.0105	21.47
mGrA	2.05	10.0	0.0184	17.16
mACI	15.05	3.13	0.0150	17.67
mGrI	3.7	3.73	0.00858	13.26

porogen, 13.5 and 13.1 nm are obtained for mACA and mACI respectively, while 1.73 and 1.72 nm pores' radii are obtained for mGrA and mGrI respectively. The atmosphere does not seem to have an effect on the pores' volume.

3.2. Contact angle measurement

Fig. 9 presents the contact angle images obtained for mACA, mGrA, mACI, and mGrI membranes. Contact angle is an important parameter that should be controlled as it influences the membrane water filtration performance and can help in predicting the fouling on the membrane's surface. The scientific community has accepted the wide definition that a surface is hydrophobic when the contact angle is > 90°, and hydrophilic if it is < 90°. All four membranes considered in this work have exhibited a contact angle less than 90° indicating that they are hydrophilic. Fig. 9a and c shows that the composite membranes mACA and mACI yield higher contact angles of 30.2 and 50.2° respectively, compared to mGrA and mGrI (Fig. 9b and d) with respective contact angle of 11.8 and 26.1°. The higher contact angle in the case of AC could be explained based on the lower decomposition temperature of AC compared to Gr, which may have contributed substantially to achieve better densification of the membrane and formation of more hydrophobic membranes. The contact angle could also be correlated with the wettability of the membranes; high contact angle is associated with lower wettability. The order of wettability of the prepared membranes could therefore be arranged as follows; mACI < mACA < mGrI < mGrA, the latter being the most wetting membrane. Chen et al. [42] found that the interfacial interaction of sludge foulant and membrane was directly related to the contact angle of water and glycerol. They demonstrated that an increase in contact angle of glycerol and water from −100 % to 100 % lead to a more repulsive monolithic membrane surface. They also found an inflexion contact angle for both solvents (76° for glycerol and 58.43° for water) where the interaction energy of the membrane with the fouling sludges became permanently negative.

Other authors [43,44] demonstrated the non-monotonic trend of the interaction energy and the contact angle, emphasizing the restraint of the concept of hydrophobicity and hydrophilicity in predicting the interfacial and fouling behavior of a membrane.
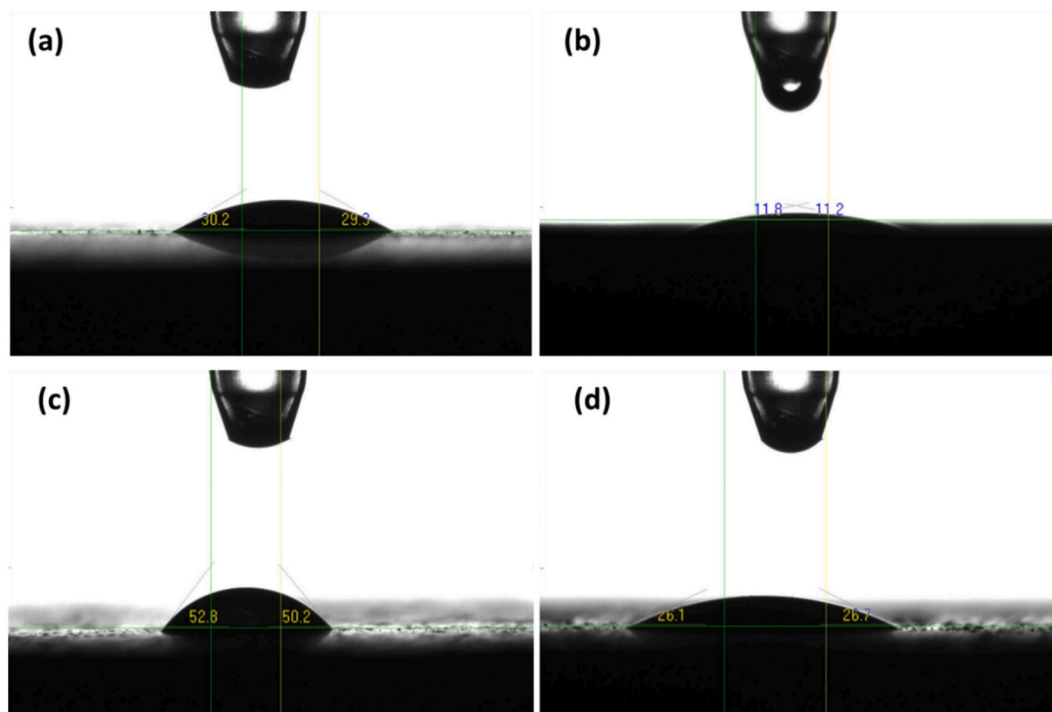

Fig. 9. Contact angle images obtained for (a) mACA, (b) mGrA, (c) mACI, and (d) mGrI membranes.

3.3. Pure water flux

The pure water flux measurements performed on mACA, mACI, mGrA, and mGrI at different operating pressures (1–3 bars) are illustrated in Fig. 10 and Table 4. The results of the study showed that the pure water fluxes increased as the operating pressure increased from 1.0 bar to 3.0 bars for the 4 membranes and remain almost constant for the duration of 60 min, however a slight decrease is noticed for mACA and mGrA shown in Fig. 10a and c. For mACA and mGrA shown in Fig. 10b and d, at pressure of 1 bar, the fluxes were 214 and 112 L h^{-1} m^{-2}. As the pressure increased to 2 bar, the fluxes increased to around 306 and 186 L h^{-1} m^{-2}, with a flux percent increase of 43 % and 66 % respectively. At 3 bars, the fluxes increased even more, reaching a value of 381 and 245 L h^{-1} m^{-2}, with almost half flux percent increases of 24.5 % and 31.7 % respectively.

For mACI and mGrI membrane, the initial fluxes were almost equal and found to be 9, and 8 L h^{-1} m^{-2}, respectively. These increased gradually to 23 and 21 L h^{-1} m^{-2}, with percent increases of 155.6 % and 162.5 %, when the pressure was increased from 1 to 2 bars. On further increase of the pressure to 3 bars, the final fluxes reached values of 78 and 77 L h^{-1} m^{-2} with respective percent increases of 239.1 % and 266.7 %. We can conclude that the membranes sintered at inert atmosphere are more suitable to be used at high pressures since they showed very high percent flux increases at these pressures compared to those sintered in air.

In general, it has been observed that the pure water fluxes for mACI and mGrI membranes are lower than those of mACA and mGrA membranes, even though the pore volumes of these two membranes are higher compared to other membranes, this justify that there is no link between the pore volumes and the flux. There must be other parameters behind this inflection such as the hydrophobicity and hydrophilicity of the membranes. This could be explained by the hydrophobic nature of these two membranes. The contact angle analysis showed that the mACI was the most hydrophobic with a contact angle of 50.2°, while mGrI yielded a contact angle of 26.1°, comparable to 30.2° of mACA, while mGrA yielded the lowest contact angle making the membrane the most hydrophilic.

Furthermore, all tested membranes were able to allow more water to flow through at higher pressures, as expected. However, a slight decrease in the flux with time is indicative that the membranes are operating perfectly well in the run time of 1 h under subcritical flux region. Critical flux is a very important parameter in operating membranes that is defined as the first flux at which the fouling starts appearing on the surface of the membrane. The decrease in the flux is usually associated with the wettability of the membranes, which can cause water to become trapped in the pores of the membrane over time.

However, it is important to note that the effect of sintering atmosphere on the performance of the clay ceramic membranes is
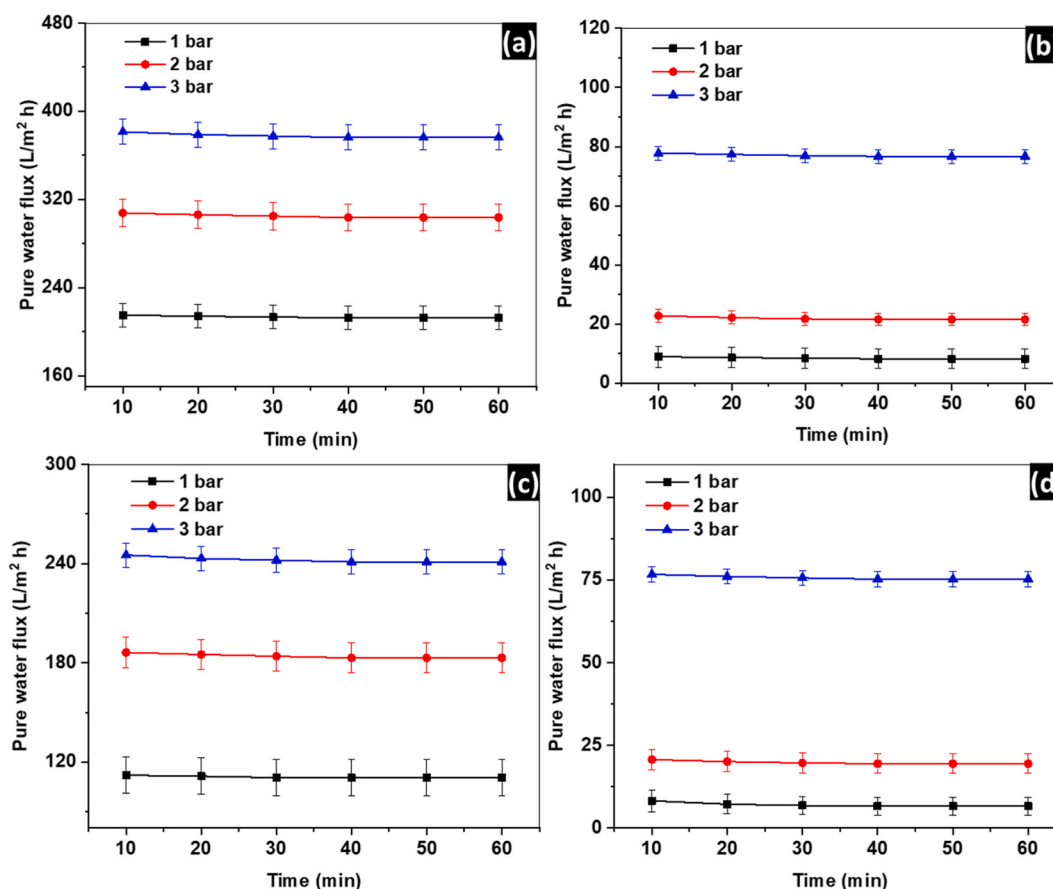

Fig. 10. Pure water flux of the fabricated ceramic membranes at different pressures. (a) mACA, (b) mACI, (c) mGrA, and (d) mGrI.

Table 4

Pure water fluxes for mACA, mGrA, mACI, and mGrI composite membranes obtained at different pressures.

Membrane	Initial Pressure (bar)	Initial water flux (L/m²h)	Final water flux (L/m²h)	% Increase
mACA	1	214	212	–
	2	306	304	43.0
	3	381	375	24.5
mGrA	1	112	110	–
	2	186	182	66.1
	3	245	240	31.7
mACI	1	9	8	–
	2	23	22	155.6
	3	78	77	239.1
mGrI	1	8	7	–
	2	21	19	162.5
	3	77	75	266.7

dependent on several factors, including the composition of the membrane and the sintering conditions. For example, the size, shape, and distribution of the AC and Gr particles can influence the degree to which they affect the porosity and permeability of the membranes.

Water flux is widely used to explain the fouling behavior of ceramic membranes since it is directly related to the surface chemistry of the membranes. For instance, the monolayer formed at the surface of a membrane when its surface is hydrophilic can facilitate the passage of water molecules through the membrane and therefore increase its water flux. Moreover, the same layer can block any probable hydrophobic pollutant and thus help increasing the fouling resistance of the membrane. Weinman et al. [45] demonstrated different antifouling behaviors of a membrane modified with zwitterion polymer, which could switch between antifouling zwitter ion and anti-microbial based on the pH change of the medium. In another study, graphene oxide (GO) modified ceramic membrane was found to have high hydrophobicity and negative surface charge which contributed to efficiently remove natural organic compounds such as humic and tannic acids as well as pharmaceuticals, the improved mechanism of removal was attributed to GO nanosheets deposited on the surface of the ceramic supports [46].

3.4. Pb^{2+} filtration flux and retention

Fig. 11 presents the evolution of lead (Pb^{2+}) permeate fluxes with time for the produced membranes, carried out under a pressure of 1 bar. High fluxes of 371 and 129 L h^{-1} m^{-2} are presented by the two membranes mACA, mGrA, compared to 70 and 13 L h^{-1} m^{-2} presented by mACI, and mGrI, respectively. The high fluxes decline parabolically with time increase to final fluxes of 270 and 91 L h^{-1} m^{-2} after 60 and 100 min working time. While low fluxes remain almost steady for the first 120 min for mACI and 60 min for mGrI, later they decline linearly to final values of 50 and 11 L h^{-1} m^{-2} after 200 and 140 min for mACI, and mGrI, respectively. Pb^{2+} fluxes are in accordance with water fluxes presented previously, with decline percentages of 27.2, 29.5, 24.3 and, 15.4 % for the mACA, mGrA, mACI, and mGrI respectively. Fluxes of pure water and water containing Pb^{2+} were found to follow different trend than the wettability of the membranes. This difference could be due to the fact that wettability is usually measured at the surface of the membrane, while the flux is actually a measuring of water permeation through the membrane which is controlled by the pores' size and volume.

The time-dependent evolution of Pb^{2+} ions retention measurement in clay membranes mixed with carbon materials and sintered under nitrogen and ambient atmospheres can provide insight into the performance and durability of these materials for potential use in heavy metals removal applications. Fig. 11a illustrates the time-dependent evolution of Pb^{2+} removal measurements through mACA. It was found that after 5 min of filtration, the Pb^{2+} retention was 94 %, indicating that the membrane was initially very effective at retaining the Pb^{2+} ions. However, the Pb^{2+} retention decreased over time, to values of about 56 % after 30 min, and 38 % after 60 min. This decrease in Pb^{2+} retention suggests that the membrane may have developed blockage of the pores by Pb^{2+} ions over time, which could have allowed the previously retained Pb^{2+} ions to escape. From 70 to 100 min, the Pb^{2+} retention appeared to have reached an equilibrium, with a retention of 33 %. This suggests that the membrane has stabilized in its ability to retain Pb^{2+} ions, but the lower retention value indicates that the membrane is less effective at retaining Pb^{2+} ions compared to the initial measurement. Fig. 11b illustrates the time-dependent evolution of Pb^{2+} retention measurement through mACI. The results show that after 10 min of filtration, the Pb^{2+} retention was almost 100 %, indicating that the membrane was very effective at retaining the heavy metal ions. This high Pb^{2+} retention suggested that the AC content in the mACI membrane increased the adsorption capability of the clay membrane for Pb^{2+} retention. The amount of AC included in the composite membrane affects the available surface area for adsorption of the Pb^{2+} heavy metal ions, as well as the porosity and stability of the membrane structure. A higher content of AC generally results in a higher adsorption capacity for heavy metal ions, as long as the physical structure of the membrane remains stable. However, the Pb^{2+} retention decreased to 92 % after 80 min, and to 75 % after 100 min, indicating a saturation of the membrane after 80 min. Fig. 11c and d illustrate the time-dependent evolution of Pb^{2+} retention for mGrA, and mGrI, respectively. The results in this case show that both membranes were able to completely remove Pb^{2+} ions over a period of 200 min, suggesting that the physical structure of the membranes was stable, and that the retention mechanism remained effective throughout the entire filtration process. The use of graphite as a component in the membrane may have contributed to the high Pb^{2+} retention, as graphite is known to have good adsorption
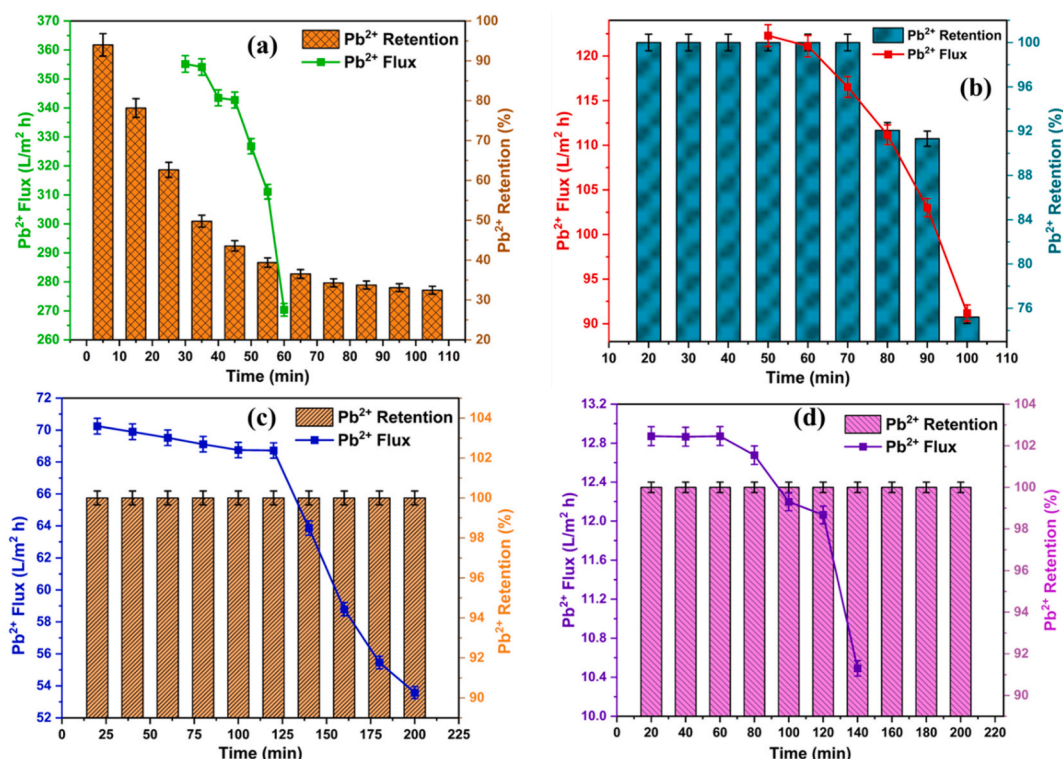
Fig. 11. Time dependent evolution of Pb^{2+} flux and retention measurements of (a) mACA, (b) mACI, (c) mGrA, and (d) mGrI membranes, under pressure P = 1 bar.

properties for heavy metal ions. The decline in the retention of Pb^{2+} when filtered over mACA and mACI membranes suggests that the mechanism of filtration is adsorption.

However, the steady state presented by mGrA and mGrI towards Pb^{2+} filtration suggests that other mechanisms are dominant such as size exclusion, which is controlled by the metal-oxygen (M − O) distance in the hydrated lead ion (Pb(OH$_2$)$_6^{2+}$), indeed the mGrA and mGrI are presented with the lowest pores' size of 1.73 and 1.72 nm respectively compared to 13.5 and 13.1 nm shown by mACA and mACI respectively. Adnane et al. [47] demonstrated previously that LTA-clay composite membrane was able to differentiate between 4 metals based on their hydrated ion size.

4. Conclusion

The present study demonstrates that largely available and cost-effective UAE local clay can be used to prepare porous ceramic membranes for removing toxic heavy metals from contaminated water. Four different ceramic membranes were prepared using activated carbon/clay and graphite/clay to get mACA and mGrA membranes and using carbon/starch/clay and graphite/starch/clay, to obtain mACI and mGrI membranes, via powder metallurgy method involving powder compaction and sintering at 1000 °C. Various analytical techniques were used for characterizing the membranes such as TGA, X-ray fluorescence, FTIR, XRD, nitrogen adsorption-desorption and FESEM. These techniques complement each other and give important information about the morphology of the membranes. Furthermore, contact angle, wettability, and water flux experiments were performed to help understand the mechanism of rejection of the heavy metal (Pb^{2+}) at the surface of the membrane. Lower water fluxes were associated with high rejection of the heavy metal due to high wettability of the membranes resulting in forming a hydrophilic monolayer at the surface of the membrane, which in turn facilitated the passage of water molecules through the membrane while stopping the water divalent hydrophobic metal pollutant. The present findings might help in understanding the mechanism of filtration of heavy metals through clay or their carbon based composite ceramic membranes. However, given the two mechanisms demonstrated by the membranes, adsorption or size exclusion, caution must be taken to explore other mechanisms of filtration such as charge repulsion between the membrane surface charge and the metal cation. To further our research, we plan to investigate the surface charge of the membranes using cyclic voltammetry to study the electrochemical surface area of the membrane and anodic stripping voltammetry to investigate the selectivity of the membranes in the presence of ionic species such as heavy metals.

Data availability statement

All data produced or investigated during this study are included in this manuscript.

CRediT authorship contribution statement

Abdelrahman K.A. Khalil: Writing – original draft, Visualization, Validation, Methodology, Investigation, Formal analysis, Data curation, Conceptualization. **Abdelaziz Elgamouz:** Writing – review & editing, Validation, Supervision, Methodology, Investigation, Conceptualization. **Saad Nazir:** Methodology, Data curation. **Muataz Ali Atieh:** Writing – review & editing, Investigation. **Hussain Alawadhi:** Methodology, Investigation, Formal analysis. **Tahar Laoui:** Writing – review & editing, Validation, Supervision, Methodology, Investigation, Conceptualization.

Declaration of competing interest

The authors declare that they have no known competing financial interests or personal relationships that could have appeared to influence the work reported in this paper.

Acknowledgements

References

[1] M.C. Reiley, Science, policy, and trends of metals risk assessment at EPA: how understanding metals bioavailability has changed metals risk assessment at US EPA, Aquat. Toxicol. 84 (2) (2007) 292–298.

[2] F.M. Pang, P. Kumar, T.T. Teng, A.K. Mohd Omar, K.L. Wasewar, Removal of lead, zinc and iron by coagulation–flocculation, J. Taiwan Inst. Chem. Eng. 42 (5) (2011) 809–815.

[3] L. Jaber, I. Ihsanullah, I.W. Almanassra, S.N. Backer, A. Abushawish, A.K. Khalil, et al., Adsorptive removal of lead and chromate ions from water by using iron-doped granular activated carbon obtained from coconut shells, Sustainability 14 (17) (2022) 10877.

[4] C. Teodosiu, A. Gilca, G. Barjoveanu, S. Fiore, Emerging pollutants removal through advanced drinking water treatment: a review on processes and environmental performances assessment, J. Clean. Prod. 197 (2018) 1210–1221.

[5] A. Kayvani Fard, G. McKay, A. Buekenhoudt, H. Al Sulaiti, F. Motmans, M. Khraisheh, et al., Inorganic membranes: preparation and application for water treatment and desalination, Materials 11 (1) (2018) 74.

[6] E.V. Shelepova, A.A. Vedyagin, Intensification of the dehydrogenation process of different hydrocarbons in a catalytic membrane reactor, Chemical Engineering and Processing-Process Intensification 155 (2020) 108072.

[7] M. Byun, H. Kim, C. Choe, H. Lim, Conceptual feasibility studies for cost-efficient and bi-functional methylcyclohexane dehydrogenation in a membrane reactor for H2 storage and production, Energy Convers. Manag. 227 (2021) 113576.

[8] M. Rezakazemi, S. Mirzaei, M. Asghari, J. Ivakpour, Aluminum oxide nanoparticles for highly efficient asphaltene separation from crude oil using ceramic membrane technology, Oil & Gas Sciences and Technology–Revue d'IFP Energies nouvelles 72 (6) (2017) 34.

[9] S.A. Younssi, M. Breida, B. Achiou, Alumina Membranes for Desalination and Water Treatment, InTech, 2018.

[10] B. Achiou, D. Beqqour, H. Elomari, A. Bouazizi, M. Ouammou, M. Bouhria, et al., Preparation of inexpensive NaA zeolite membrane on pozzolan support at low temperature for dehydration of alcohol solutions, J. Environ. Chem. Eng. 6 (4) (2018) 4429–4437.

[11] G.M. Alwan, A.A. Alwasiti, Improving the performance of a catalytic membrane reactor via stochastic optimization, Int.Rev.Chem.Eng 5 (2013) 156–171.

[12] X. Zheng, Z. Zhang, D. Yu, X. Chen, R. Cheng, S. Min, et al., Overview of membrane technology applications for industrial wastewater treatment in China to increase water supply, Resour Conserv Recycling 105 (2015) 1–10.

[13] W. Lau, G. Lai, J. Li, S. Gray, Y. Hu, N. Misdan, et al., Development of microporous substrates of polyamide thin film composite membranes for pressure-driven and osmotically-driven membrane processes: a review, J. Ind. Eng. Chem. 77 (2019) 25–59.

[14] Z. He, Z. Lyu, Q. Gu, L. Zhang, J. Wang, Ceramic-based membranes for water and wastewater treatment, Colloids Surf Physicochem Eng Aspects 578 (2019) 123513.

[15] S.R.H. Abadi, M.R. Sebzari, M. Hemati, F. Rekabdar, T. Mohammadi, Ceramic membrane performance in microfiltration of oily wastewater, Desalination 265 (1–3) (2011) 222–228.

[16] S.A. Alftessi, M.H.D. Othman, M.R. Adam, T.M. Farag, A.F. Ismail, M.A. Rahman, et al., Novel silica sand hollow fibre ceramic membrane for oily wastewater treatment, J. Environ. Chem. Eng. 9 (1) (2021) 104975.

[17] A.M. Al Amer, T. Laoui, A. Abbas, N. Al-Aqeeli, F. Patel, M. Khraisheh, et al., Fabrication and antifouling behaviour of a carbon nanotube membrane, Mater. Des. 89 (2016) 549–558.

[18] H.K. Shahzad, M.A. Hussein, F. Patel, N. Al-Aqeeli, M.A. Atieh, T. Laoui, Synthesis and characterization of alumina-CNT membrane for cadmium removal from aqueous solution, Ceram. Int. 44 (14) (2018) 17189–17198.

[19] F. Patel, M. Khraisheh, M.A. Atieh, T. Laoui, Novel aluminum oxide-impregnated carbon nanotube membrane for the removal of cadmium from aqueous solution, Materials 10 (10) (2017) 1144.

[20] J. Kujawa, S. Cerneaux, W. Kujawski, Investigation of the stability of metal oxide powders and ceramic membranes grafted by perfluoroalkylsilanes, Colloids Surf Physicochem Eng Aspects 443 (2014) 109–117.

[21] T. Wu, N. Wang, J. Li, L. Wang, W. Zhang, G. Zhang, et al., Tubular thermal crosslinked-PEBA/ceramic membrane for aromatic/aliphatic pervaporation, J. Membr. Sci. 486 (2015) 1–9.

[22] A. Elgamouz, N. Tijani, From a naturally occurring-clay mineral to the production of porous ceramic membranes, Microporous Mesoporous Mater. 271 (2018) 52–58.

[23] A. Elgamouz, N. Tijani, Dataset in the production of composite clay-zeolite membranes made from naturally occurring clay minerals, Data Brief 19 (2018) 2267–2278.

[24] F. Patel, M.A. Baig, T. Laoui, Processing of porous alumina substrate for multilayered ceramic filter, Desalination Water Treat. 35 (1–3) (2011) 33–38.

[25] B. Achiou, H. Elomari, M. Ouammou, A. Albizane, J. Bennazha, A. Aaddane, et al., Study of added starch on characteristics of flat ceramic microfiltration membrane made from natural Moroccan pozzolan, J. Mater. Environ. Sci. 9 (2018) 1013–1021.

[26] A. El-Kordy, A. Elgamouz, E.M. Lemdek, N. Tijani, S.S. Alharthi, A. Kawde, et al., Preparation of sodalite and faujasite clay composite membranes and their utilization in the decontamination of dye effluents, Membranes 12 (1) (2022) 12.

[27] Y.N. Vodyanitskii, N.P. Kirillova, D.V. Manakhov, M.M. Karpukhin, Iron compounds and the color of soils in the Sakhalin island, Eurasian Soil Sci. 51 (2) (2018) 163–175.

[28] A. El-Kordy, A. Elgamouz, E.M. Lemdek, N. Tijani, S.S. Alharthi, A. Kawde, et al., Preparation of sodalite and faujasite clay composite membranes and their utilization in the decontamination of dye effluents, Membranes 12 (1) (2021) 12.

[29] A. Elgamouz, N. Tijani, I. Shehadi, K. Hasan, M. Al-Farooq Kawam, Characterization of the firing behaviour of an illite-kaolinite clay mineral and its potential use as membrane support, Heliyon 5 (8) (2019) e02281.

[30] I. Kim, J. Lee, J. An, E. Jung, H. Lee, M. Morita, et al., Capacity improvement of tin-deposited on carbon-coated graphite anode for rechargeable lithium ion batteries, Int. J. Electrochem. Sci. 11 (2016) 5807–5818.

[31] M. Nakagawa, M. Santosh, S. Yoshikura, M. Miura, T. Fukuda, A. Harada, Kaolin deposits at melthonnakkal and pallipuram within trivandrum block, southern India, Gondwana Res. 9 (4) (2006) 530–538.

[32] R.L. Frost, E. Mendelovici, Modification of fibrous silicates surfaces with organic derivatives: an infrared spectroscopic study, J. Colloid Interface Sci. 294 (1) (2006) 47–52.

[33] A. Elgamouz, N. Tijani, From a naturally occurring-clay mineral to the production of porous ceramic membranes, Microporous Mesoporous Mater. 271 (2018) 52–58.

[34] D. Lahcene, A. Behilil, B. Zahraoui, H. Benmehdi, M. Belhachemi, A. Choukchou-Braham, Physicochemical characterization of new natural clay from south west of Algeria: application to the elimination of malachite green dye, Environ. Prog. Sustain. Energy 38 (4) (2019) 13152.

[35] H. Othmani-Assmann, M. Benna-Zayani, S. Geiger, B. Fraisse, N. Kbir-Ariguib, M. Trabelsi-Ayadi, et al., Physico-chemical characterizations of Tunisian organophilic bentonites, J. Phys. Chem. C 111 (29) (2007) 10869–10877.

[36] S. Arellano-Cardenas, T. Gallardo-Velazquez, G.V. Poumian-Gamboa, G. Osorio-Revilla, S. Lopez-Cortez, Y. Rivera-Espinoza, Sorption of naringin from aqueous solution by modified clay, Clays Clay Miner 60 (2) (2012) 153–161.

[37] R.L. Frost, E. Mendelovici, Modification of fibrous silicates surfaces with organic derivatives: an infrared spectroscopic study, J. Colloid Interface Sci. 294 (1) (2006) 47–52.

[38] A. Elgamouz, N. Tijani, I. Shehadi, K. Hasan, M.A. Kawam, Characterization of the firing behaviour of an illite-kaolinite clay mineral and its potential use as membrane support, Heliyon 5 (8) (2019) e02281.

[39] M. Nakagawa, M. Santosh, S. Yoshikura, M. Miura, T. Fukuda, A. Harada, Kaolin deposits at melthonnakkal and pallipuram within trivandrum block, southern India, Gondwana Res. 9 (4) (2006) 530–538.

[40] K.S. Sing, R.T. Williams, Physisorption hysteresis loops and the characterization of nanoporous materials, Adsorpt. Sci. Technol. 22 (10) (2004) 773–782.

[41] T. Li, Powder injection molding of metallic parts and structures, in: F.G. Caballero (Ed.), Encyclopedia of Materials: Metals and Alloys, Elsevier, Oxford, 2022, pp. 401–416.

[42] J. Chen, L. Shen, M. Zhang, H. Hong, Y. He, B. Liao, et al., Thermodynamic analysis of effects of contact angle on interfacial interactions and its implications for membrane fouling control, Bioresour. Technol. 201 (2016) 245–252.

[43] L. Chen, Y. Tian, C. Cao, J. Zhang, Z. Li, Interaction energy evaluation of soluble microbial products (SMP) on different membrane surfaces: role of the reconstructed membrane topology, Water Res. 46 (8) (2012) 2693–2704.

[44] N. Subhi, A.R.D. Verliefde, V. Chen, P. Le-Clech, Assessment of physicochemical interactions in hollow fibre ultrafiltration membrane by contact angle analysis, J. Membr. Sci. 403–404 (2012) 32–40.

[45] S.T. Weinman, M. Bass, S. Pandit, M. Herzberg, V. Freger, S.M. Husson, A switchable zwitterionic membrane surface chemistry for biofouling control, J. Membr. Sci. 548 (2018) 490–501.

[46] K.H. Chu, M. Fathizadeh, M. Yu, J.R. Flora, A. Jang, M. Jang, et al., Evaluation of removal mechanisms in a graphene oxide-coated ceramic ultrafiltration membrane for retention of natural organic matter, pharmaceuticals, and inorganic salts, ACS Appl. Mater. Interfaces 9 (46) (2017) 40369–40377.

[47] A. Lahnafi, A. Elgamouz, N. Tijani, L. Jaber, A. Kawde, Hydrothermal synthesis and electrochemical characterization of novel zeolite membranes supported on flat porous clay-based microfiltration system and its application of heavy metals removal of synthetic wastewaters, Microporous Mesoporous Mater. 334 (2022) 111778.